2010

Designing Of Energy Efficient Indoor Environments Using A Localized Radial Basis Function Meshless Method

Victor Huayamave
University of Central Florida

Showcase of Text, Archives, Research & Scholarship

DESIGNING OF ENERGY EFFICIENT INDOOR ENVIRONMENTS USING A LOCALIZED RADIAL BASIS FUNCTION MESHLESS METHOD

by

VICTOR A. HUAYAMAVE
B.S. University of Central Florida, 2008

A thesis submitted in partial fulfillment of the requirements
for the degree of Master of Science
in the Department of Mechanical, Materials, and Aerospace Engineering
in the College of Engineering and Computer Science
at the University of Central Florida
Orlando, Florida

Summer Term
2010

Major Professor: Eduardo A. Divo

ABSTRACT

Around the world, the energy over consumption issue has been one of the key socio-economic and political challenges, which has drastically worsened over the last few years. Over the years engineers and environmentalists have proposed several approaches to improve energy efficiency. One is to reduce energy demand by improving consumption habits and a second approach is to introduce the use of a "greener" concept by using biomaterials in a diverse and more efficient manner in engineering construction to create energy efficient environments. This work will investigate the effects of using "green" stabilized earth materials to provide and enhance thermal regulation for indoor environments. This effects can be compared to what skin does to regulate body temperature in humans, animals, and plants. On this effort the thermal behavior of several biomaterials will be analyzed using a computational tool in order to test the mechanical properties of biomaterials and also several geometry configurations to minimize the energy needed for heating and cooling an environment. In this research a localized radial basis function (LRBF) meshless method, developed by the Computational Mechanics Lab (CML) at the University of Central Florida, has been implemented to test several wall geometrical configuration using known biomaterials such as clay. The advantage of using the LRBF meshless method in this particular research is based in the accuracy of the numerical method and also because it decreases computation time regardless of model complexity geometry without the need of mesh generation. This research

includes a complete description of the LRBF meshless method, as well as a quantification of cooling methods that have been used by past civilizations and recent construction standards but have not been validated on scientific basis. Results are presented which will demonstrate the effectiveness of using integrated sheets of biomaterials in engineering construction to increase energy efficiency in indoor environments.

To all my family and friends who encouraged me so much not only in my academic career

but also in life and helped me become the person I am today.

ACKNOWLEDGMENTS

Special thanks to:

TABLE OF CONTENTS

LIST OF FIGURES

LIST OF TABLES

CHAPTER 1
INTRODUCTION

The concept of energy efficient indoor environments (EEIE) has been used by past civilizations, especially in arid territories, to help them protecting against harsh climate conditions. However there was not any quantification or scientific method used by these civilizations to design EEIE. It is the intent of this research to give a scientific validation using a computational tool to evaluate the heat transfer and to prove the concept using biomaterial to improve energy efficiency. Also in the analysis it is desire to see if the use of biomaterials minimizes temperature fluctuations in indoor environments. A notorious example of this process is the evaporation from skin of sweat generated by the thermoregulatory system of the body to provide cooling in such a biological system.

Traditional numerical techniques such as the finite element method (FEM) [1] and the finite volume method (FVM) [2] have been proposed to solve multiphysics problem, such as the one we have in hand, but they require significant effort when it comes to the generation of structured point distribution or so-called mesh. Mesh generation in these methods is very tie consuming and often the mesh has to be adapted to the solution. The work presented in this effort proposes the use of a LRBF meshless method to solve the heat transfer interaction in the designing of EEIE using biomaterials. Although the use of this method has been kept at the research level, its validity has been demonstrated in several applications including solid mechanics [1] , fluid dynamics [2], and heat transfer [3, 4, 5].

Specially, this research implements the LRBF meshless method to analyze the heat transfer between biomaterials, engineering construction materials, and indoor environment taking into account all the different heat transfer modes. The following research report will detail the implementation of the LRBF meshless method and verification of this approach, as well as demonstrate its effectiveness in the designing of EEIE.

In order to understand the benefits of using the LRBF methods and biomaterials in the designing of EEIE, a reasonable understanding of the numerical method implemented and biomaterials is needed. Therefore, Chapters 2 and 3 provides a through discussion of the history and relevant background information in the LBRF meshless method and the used biomaterials in construction. Chapter 2 is devoted to providing an explanation of different biomaterial properties and how they can be used as engineering construction materials. This particular Chapter will illustrate and bring to light the goals of using biomaterials as construction materials for the designing of EEIE and also will highlight the latest reseach and development made on this fiels. In the same fashion, Chapter 3 will introduce the theory behind the LRBF Meshless Method, which as it has been mentioned has advantages over several methods which has been used in commercial software packages. It is intended that these two first chapters are detailed enough so that the remainder of this work may be followed by discussing specific applications and scenarios where RLBF Meshless Method can be used to solve the heat transfer problem in the designing of EEIE using biomaterials. Following this background information, the specific details to solve the problem in hand will be presented in Chapter 4. This Chapter in particular is divided into several apporpriate sections to discuss the methodology used to solve the coupled heat transfer problem and to

specify the configurations that will be used for this research. Chapter 4 will also provide information and data for initial testing to be used to simulate several scenarios of EEIE. After this description of the research methodology, the problem is quantified by presentation of several example scenarios in Chapter 5. These examples demonstrate the application of these techniques within the context of solving the coupled heat transfer problem using the LRBF Meshless Method. These examples include a comparison of different earth-based, organic, and standard materials to understand how EEIE can be designed with the use of the LRBF Meshless Method. This report then concludes with a thorough discussion of the observations and findings of this research effort in Chapter 6, including final remarks regarding avenues of exploration for future research within the field.

CHAPTER 2
THERMOREGULATORY BIOMATERIALS AS
CONSTRUCTION MATERIALS

Stabilized or rammed earth is used since prehistoric times as the dominant construction material, particularly in arid countries. Its history as a construction material is much longer than that of fired clay bricks. As much as the research community would like to take the ownership of the discovery of stabilized earth in so far as the thermal regulation is concerned, the evolutionary knowledge of humans points out that all past civilizations used earthen elements either overlain by coconut palm leaves or reinforced by straw or husk [6, 7, 8, 9]. A cursory look at the earth constructions throughout the world humbles the engineering community with regard to the extent it continues to be accepted by the local communities. However, much of the earth-based construction appears to suffer from lack of scientific basis. The vast number of structures made of stabilized earth wall in almost all continent, and the use of leaves, either integrated within or layered on top, has not attracted the attracted the attention of every research community thus far.

Apart from the obvious advantages of mud blocks, natural and environmentally sustainable materials and low cost, earth-enclosed environments offer remarkable stability in temperatures. In climates with hot days and cold nights, temperatures inside earth houses varied only by 4°C; in the concrete house, the variation was 16°C [10]. Researchers worldwide reported similar results [6, 11]. Anecdotal evidence presented by one researcher indicates that

temperatures inside a 'mud' house remained fairly constant at 25ºC with the exterior air temperatures varying from 14ºC to 35ºC; the interior air temperature of a concrete building with the same exterior condition varied from 22ºC to 40ºC.

In the face of such convincing anecdotal evidence, literature is surprisingly scanty when it comes to formal scientific studies on the heat transfer and transport in stabilized soils, and practically non-existent in the area of reverse-engineering soil materials to fulfill desired thermal regulation. Figure 2.1 shows a typical example of how earth-based and organic materials are layered together to fulfill desired thermal regulation and to improve the design of energy efficient indoor environments (EEIE).
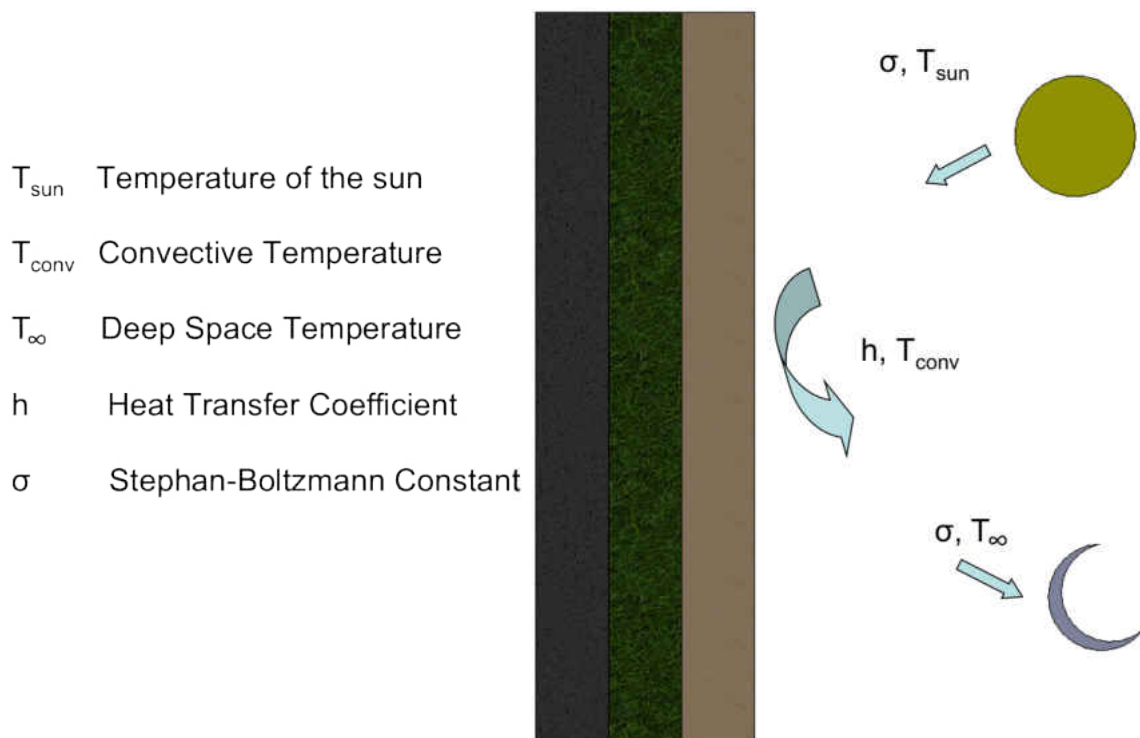

Figure 2.1: Layered combination of earth-based and organic materials under typical ambient cycling conditions

Soil sciences have seen rapid growth in understanding thermal properties of soils in an agronomical context; however, geotechnical studies of the heat flow through engineered soils are very few. The few studies reported on thermal regulation of stabilized earthen wall attempted to develop correlations between density and thermal conductivity [7, 12]. Heat conduction in soils is generally viewed as dependent on particle-to-particle contact and the formation of water bridges [13, 14]. Increase of thermal conductivity with increasing bulk density is attributed to a greater contact between primary particles, which increases the continuity of the solid phase. The effect of soil bulk density appears to be more pronounced at high water contents [15].

2.1   Plant leaves and human skin as thermoregulatory systems

In contrast to stabilized earth materials, plant leaves and animal skin were thoroughly studied for their thermoregulatory properties. Both human body and plant leaves share a common principle of cooling. Evaporation from leaves and perspirations from human body, both of which require energy, cause cooling to these biological systems. Sensible heat loss and evaporative heat loss are the most important processes in the regulation of leaf temperature, and the ratio of the two is called Bowen ratio [16, 17]. Plant systems with very high Bowen ratios conserve water but have to endure very high leaf temperatures in order to maintain a sufficient temperature gradient between the leaf and the air. When Bowen ratios approach zero, heat dissipation is due mostly to evaporative heat lost such as in the case of lawns on a relatively still day. Evaporation rates for entire canopies can be calculated using

6

measurements of the Bowen ratio, net incident radiation, the heat loss from the soil, and the gradients in temperature and water vapor concentration above the canopy [18]. Plant physiology has progressed to advanced stages of using these theoretical concepts, often in the context of agronomy; however, plant systems incorporated in cementitious construction materials were not researched from such basic principles. Instead, mechanical properties of the plant-integrated materials, and deterioration of plant tissues, occupied the attention of construction engineers. Excellent examples are development of lightweight cement boards using coconut coir [19], deterioration of coconut leaf thatches under natural and accelerated environmental conditions [20], thermal degradation of banana and coconut fibers [21], and hydration characteristics of cement-bonded composites made from rattan cane and coconut husk [22].

Sweat rates through perspiring glands and the associated changes in skin temperature are well addressed in literature related to applied physiology and environmental medicine. Out of the vast literature on this theme, it is found that the studies relating sweat rate and skin temperature in hot climates to be especially relevant to the proposed research. As an example, the exponential relationships proposed between the mean sweat rate and mean skin temperature in heat budgets of cattle [23], provide important tools to explore analogies between animal skin and plant leaves, and set the stage for conceptualization and design of Geodermis (System of soils and plan-based materials that provide thermal regulation for indoor environments). Figure 2.2 shows the concept behind Geodermis and also illustrates some examples of how earth-based and plant-based layered materials can be employed for the designing of energy efficient environment.
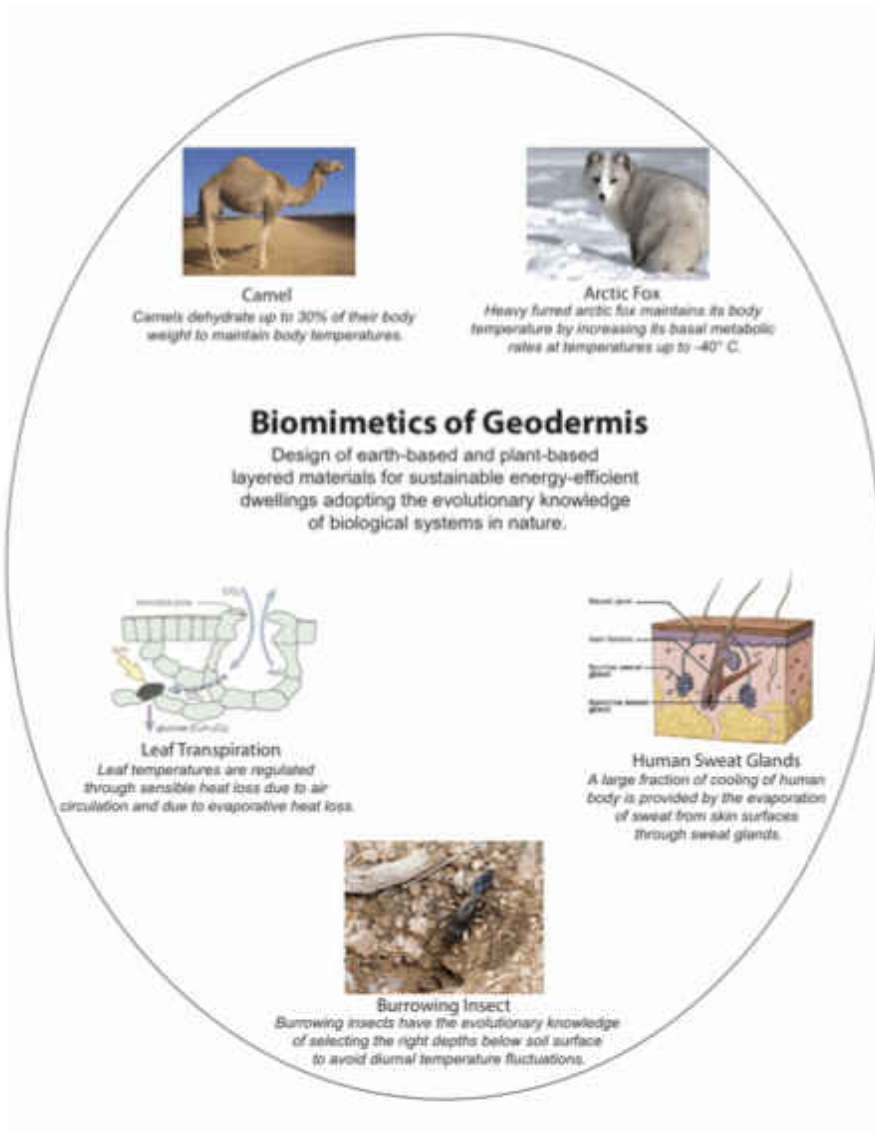
Figure 2.2: Geodermis Concept Illustration

In the case of humans, the conditions required to initiate sweating in terms of environmental temperature [24], and the influence of the rate of change in temperature of sweating [25] provides some of the earliest concepts on the role of human skin as a thermoregulatory system. Since these earlier studies, applied physiology has seen predictive formulae and equations relating sweat lost to specific work loads, climates, clothing ensembles, and fluctuating

thermal conditions [26, 27]. The literature is advanced enough that solutions now exist even for such specific problems as relating heat loss through skin during underwater work and water exercises [28, 29]. Recent studies have gone so far as to attempt mechanical models of skin providing insights on how the stratum corneum, the outermost layer of the skin, provides the body with a physiologically essential barrier to unregulated water loss and the influx of exogenous substances. It is interesting from a construction-engineering standpoint how the stratum corneum displays both mechanical cohesion as well as thermal integrity at the same time.

CHAPTER 3
LRBF MESHLESS METHOD

While finite element methods (FEM) and finite volume methods (FVM) have been developed to a mature stage such that they are now utilized routinely to model complex multiphysics problems, the both require significant effort in mesh generation. Meshless methods are a relative newcomer to the field of computational methods and have recently attracted much interest as they offer the hope of reducing the effort devoted to model preparation [30, 31, 32, 33, 1, 34, 35]. The approach find its origin in classical spectral or pseudo-spectral methods [36, 37, 38, 39, 40, 41] that are based on global orthogonal functions such as Legendre or Chebyshev polynomials requiring a regular nodal point distribution. In contrast, meshless methods use a nodal or point distribution that is not required to be uniform or regular due to the fact that most such techniques rely on global radial-basis functions (RBF) [42, 43, 44, 45]. RBF have proved to be quite successful in their application to a series of global meshless methods [46, 47, 48, 49, 50, 51], however, these techniques can also be computationally intensive. Recently, the localized meshless method [52, 53, 54] have been proposed to address many of the issues posed by global meshless methods. A LRBF collocation method based on the Hardy Multiquadrics RBF [45] has been developed using polynomial-augmented RBF [55, 56, 3, 57, 58] employed for the expansion of the problem variables. The formulation provides substantial computational saving over traditional meshless methods and mitigates the issues of oscillative derivative fields around large gradient areas.

The LRBF meshless method will be employed in this study as the method of choice for solving the field problem in hand that arises as result of a designed geometrical configuration and thermal property distribution of a composite wall. First a domain will be defined using typical standards for the construction of composite walls and then thermal effects due to conduction, natural convection and forced convection will be quantified by solving the problem using the LRBF approach.

3.1 LRBF Meshless Formulation

To begin the meshless formulation, a set of data centers (NC) is defined over a region composed of a domain and a boundary. The region containing the data centers is composed of boundary points (NB) and inside points (NI). Figure 3.1 show how typically internal points and boundary points are distributed in a defined domain and its boundary.
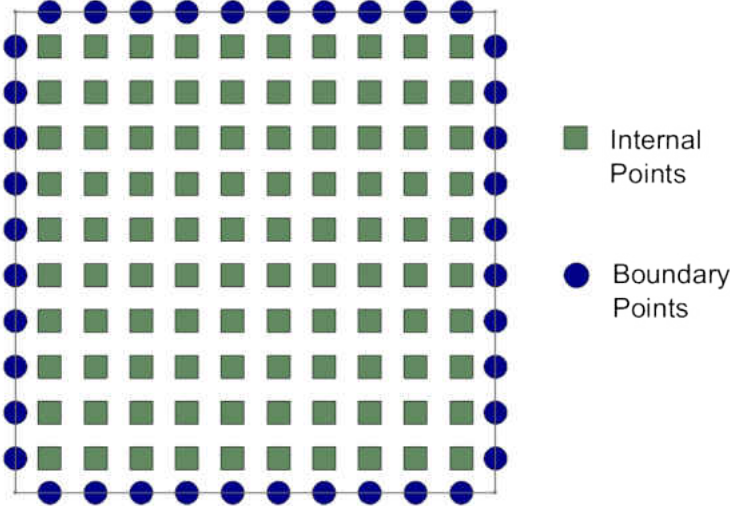

Figure 3.1: Collocation of Boundary Points and Internal Points over a defined Region

The main difference between boundary points and the internal points is that the generalized boundary conditions equation is applied at the first, while the governing equation is applied at the last. The following relation shows how the expansion over a group of influence points, N, is found

$$\phi(x) = \sum_{j=1}^{N} \alpha_j \chi_j(x) + \sum_{j=1}^{NP} \chi_{j+N} P_j(x) \qquad (3.1)$$

where in the first term of Equation 3.1 N is the total number of points in the domain, α are the expansion coefficients for ϕ, and $\chi(x)$ is a predefined expansion function. Furthermore, a similar expression appears in the second term of Equation 3.1 which is a similar expansion performed over NP number of polynomial function, $P_j(x)$, which guarantees that constant and linear fields can be retrieved exactly. Equation 3.1 assumes a global collocation, which, has been stated as a non ideal method. Therefore, instead assuming a global collocation the domain can be separated into small regions called local topologies meaning that instead of solving over the entire domain, the problem is solved by applying the basis function only to local topologies. Equation 3.1 is reformulated to solve for an interpolated field having the following form

$$\phi(x) = \sum_{j=1}^{NF} \alpha_j \chi_j(x) + \sum_{j=1}^{NP} \chi_{j+NF} P_j(x) \qquad (3.2)$$

where NF is the number of points in a given local topology. Figure 3.2 shows a typical representation of a topology. By looking at the local topology represented by Ω_i, it can be seen in this particular topology for the given data center NF is equal to five.
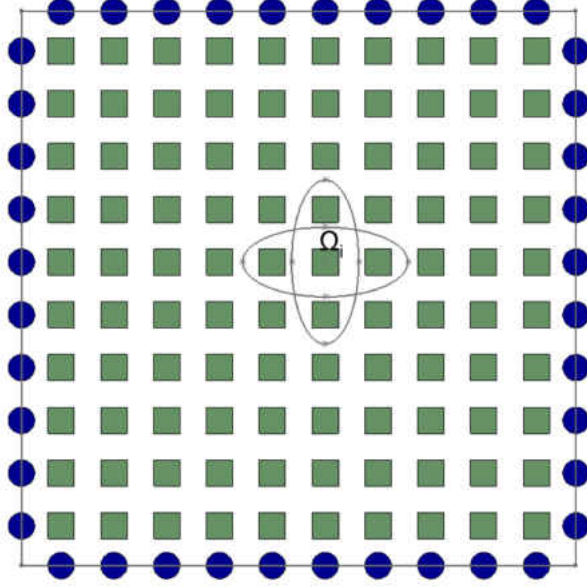
Figure 3.2: Topology Representation on a defined Domain

The Helmholtz potential ϕ in this particular case is illustrated and the same form is directly generalized for all other field variables. The NF expansion functions may be written in terms of radial-basis interpolation functions, in particular from the family of the so-called Inverse Hardy Multiquadrics[45], where n=1 and it has the following form

$$\chi_j(x) = \frac{1}{\sqrt{r_j^2(x) + c^2}} \tag{3.3}$$

where $r_j(x)$ is the Euclidean distance evaluated by

$$r_j(x) = \| x - x_j \| \tag{3.4}$$

and c is a shape parameter. For a specific expansion over a specific set of data centers, smoother derivative fields are retrieved using a large value for the shape parameter. However, as it can be seen in Equation 3.3, increasing c will cause the function to become flatter. This type of behavior will caused the function to become ill-conditioned and the system will

become singular. Because of this, a simple optimization search is employed to determine a specific value for the shape parameter c that is used in each expansion over the different local topologies that cover the entire field. Therefore, c cannot be a constant over the entire field, instead it takes on a different value in every local topology such ill-conditioning of the data center collocation matrix is avoided. In the literature[48, 51, 59, 60] it is found that the best interpolation is achieved when the conditioning number of the system oscillates between 10^{10} and 10^{12}. Also it is important to noticed that the optimization of the c is crucial when complex geometry in is analyzed to obtain accurate interpolation behavior. This approach reduces the burden of the more common interpolation methods by expanding the field variable locally around each data center to obtain its derivatives, which are used in the explicit time-marching schemes already described. Selecting an influence region or a localized topology of expansion around each data center is easily accomplished by a circular search around each data center. The real advantage of the localized collocation approach is capitalized in the way the derivatives at the center of the topology are calculated.

The collocation of the known field variable ϕ at the points within the localized topology, lead to the following expression in matrix-vector form

$$\{\phi\} = [G]\{\alpha\} \tag{3.5}$$

Equation 3.5is a simplified version of Equation 3.2 which needs to be solved for the expansion coefficients α

$$\{\alpha\} = [G]^{-1}\{\phi\} \tag{3.6}$$

where $[G]^{-1}$and $[\phi]$ are composed by

14

$$[G] = \begin{bmatrix} \chi_1(x_1) & \cdots & \chi_{NF}(x_1) & P_1(x_1) & \cdots & P_{NP}(x_1) \\ \chi_1(x_2) & \cdots & \chi_{NF}(x_2) & P_1(x_2) & \cdots & P_{NP}(x_2) \\ \vdots & \vdots & \vdots & \vdots & \vdots & \vdots \\ \chi_1(x_{NF}) & \cdots & \chi_{NF}(x_{NF}) & P_1(x_{NF}) & \cdots & P_{NP}(x_{NF}) \\ P_1(x_1) & \cdots & P_1(x_{NF}) & 0 & \cdots & 0 \\ \vdots & \vdots & \vdots & \vdots & \vdots & \vdots \\ P_{NP}(x_1) & \cdots & P_{NP}(x_{NF}) & 0 & \cdots & 0 \end{bmatrix} \tag{3.7}$$

$$\{\phi\} = \begin{pmatrix} \phi(x_1) \\ \phi(x_2) \\ \vdots \\ \phi(x_{NF}) \\ 0 \\ \vdots \\ 0 \end{pmatrix}$$

The interest of the LRFB method is based in the development of the weight representing a particular derivative at the data center. Therefore the localized expansion equation can be expressed such that it estimates field variable derivatives at the data center

$$\phi(x_c) = \sum_{j=1}^{N} \alpha_j \chi_j(x_c) + \sum_{j=1}^{NP} \chi_{j+N} P_j(x_c) \tag{3.8}$$

where x_c is the data center of the topology, resulting in the matrix-vector form

$$\phi(x_c) = \{\chi(x_c)\}^T \{\alpha\} \tag{3.9}$$

where the vector {Lc} is composed by

$$\phi\left(x_c\right) = \{\chi\left(x_c\right)\}^T \left[G\right]^{-1} \{\phi\}$$ (3.10)

Equation 3.10 can be used to interpolate any data center lying in the region of interest. The fact that field variables and their derivative can be estimated by simpler inner products of vectors by using the localized collocation method makes this approach an attractive option. Another feature of this method is that the memory functions of this approach are minimal, as no global collocation matrix is allocated, and only very small vectors are stored for every one of the data centers.

3.2 Virtual RBF Finite Difference Collocation

Conventional finite difference collocation techniques involve truncating the Taylor series expansion to approximate a given derivative at a specific location within a field. The finite difference formulations can therefore be directly applied to any regular point distribution when the surrounding nodes are properly located within the bounds of the approximation. However, this technique has a limitation in that it requires a regular, defined distribution of nodes, something that is not possible for an unstructured, meshless domain. By utilizing some of the concepts of Localized Radial Basis collocation, the standard finite difference formulation can be extended to non-regular node distributions and be made into a meshless technique. The first step to formulating the Virtual RBF Finite Difference technique is to understand the concepts behind native finite differencing. As already stated, the underlying

concept is to truncate the Taylor series representation of the derivatives at a given location to produce approximate values that can be evaluated with acceptable error.

3.3   Smoothing Scheme using Moving Least Squares

When formulating direct derivative expansion vectors within each topology, care must be taken since odd one-sided derivatives tend to oscillate towards areas of large gradients, like in recirculating zones, corners and impingent planes. There's an effective method consisting of the application of moving least-squares smoothing or MLSS over the data center topology to approximate the derivative value at the data center. This MLSS application can be extended to be formulated in the same form a value at the data center can retrieved by a simple inner product of a vector that can be prebuilt and stored and the vector of field variable values in the topology. Consider the following topology around the data center xc

[figure]

On this particular case a field $\phi(x)$ using NP polynomials $P_j(x)$ may be formulated such that

$$\phi(x) = \sum_{j=1}^{NP} \alpha_j P_j(x) \tag{3.11}$$

Using a least squares minimization process the expansion coefficients are found over all the influence points NF yielding to

$$\sum_{j=1}^{NP} \alpha_j \left[\sum_{k=1}^{NF} P_i(x_k) P_j(x_k) \right] = \sum_{k=1}^{NF} P_i(x_k) \phi(x_k) \tag{3.12}$$

or in matrix vector form

$$[c]_{NPxNP} \{\alpha\}_{NPx1} = [P]_{NPxNF} \{\phi\}_{NFx1} \tag{3.13}$$

so the expansion coefficients are

$$\{\alpha\}_{NPx1} = [C]^{-1}_{NPxNf} [P]_{NPxNF} \{\phi\}_{NFx1} \tag{3.14}$$

where the least-squares coefficient matrix $[C]_{NPxNP}$ of elements $[C]$ is

$$C_{ij} = \left[\sum_{k=1}^{NF} P_i(x_k) P_j(x_k) \right] \tag{3.15}$$

and after expansions and reductions, the least-squares operator vector is built explicitly

as

$$\{\mathcal{L}_{ls}\}^T_{1xNF} = \{\mathcal{L}P_c\}^T_{1xNP} [C]^{-1}_{NPxNP} [P]_{NPxNF} \tag{3.16}$$

This smoothing scheme is performed over the same topology as the localized RBF collocation. Least-squares operator vectors can be prebuilt at the same preprocessing stage as the topology generation, shape parameter optimization, and RBF collocation. The moving least-squares smoothing scheme is implemented to approximate the convective derivatives of the momentum and energy equation to add stability to the iteration process.

CHAPTER 4
METHODOLOGY

4.1 Formulation of Governing Equations

The Navier-Stokes equations govern the transient incompresible fluid flow. The equations in non-conservative form showing the conservation of linear momentum, mass and energy, assuming the fluid is Newtonian, are shown a follows

$$\nabla \cdot \overrightarrow{V} = 0 \tag{4.1}$$

$$\rho \frac{\partial \overrightarrow{V}}{\partial t} + \rho(\overrightarrow{V} \cdot \nabla)\overrightarrow{V} = -\nabla p_t + \mu \nabla^2 \overrightarrow{V} + \rho \overrightarrow{g} + \rho \overrightarrow{f} \tag{4.2}$$

$$\rho c \frac{\partial T}{\partial t} + \rho c(\overrightarrow{V} \cdot \nabla)T = k\nabla^2 T + \Phi \tag{4.3}$$

where, $\overrightarrow{V}$ is the flow vector, ρ is the bulk density of the flow, p_t is the pressure field, μ is the absolute fluid viscosity $\overrightarrow{g}$ is the gravitational acceleration field, $\overrightarrow{f}$ is the specific body force, c is the fluid specific heat, T is the field temperature, k is the fluid thermal conductivity, and Φ is the nonlinear dissipation term. These terms are all functions of space (x) and time (t) in a fixed domain Ω surrounded by a closed boundary Γ. For simpler notation, the explicit space-time dependency of each dependent variable has been omitted. There are also certain variations on the above-mentioned equations. If the flow is buoyancy-driven, the pressure field p_t in Equation 4.2 can be expanded in terms of hydrostatic pressure p_h and the motion pressure p as $p_t = p_h + p$. The hydrostatic pressure gradient can be expanded as

well by hydrostatic consideration, in terms of the gravitational field and the density at rest as $\nabla p_h = \rho_o \vec{g}$ resulting in the following momentum equation

$$\rho \frac{\partial \vec{V}}{\partial t} + \rho(\vec{V} \cdot \nabla)\vec{V} = -\nabla p + \mu \nabla^2 \vec{V} + \vec{g}(\rho - \rho_o) + \rho \vec{f} \qquad (4.4)$$

The gravitational term from the previous resulting equation can be simplified by Boussinesq approximation

$$(\rho - \rho_o) = \rho\beta(T_o - T) \qquad (4.5)$$

Here, β is thermal expansion coefficient of the fluid and T_o is the temperature of the fluid at rest, or the reference temperature.

It has been proven that this approximation works when dealing with natural-convective flows when the temperature variation, $(T_o–T)$ is less than $1/\beta$. It can also be demonstrated that for ideal gases and a constant value for incompressible liquids, $\beta = 1/T$. The momentum equation results as follows after using Boussinesq approximation

$$\rho \frac{\partial \vec{V}}{\partial t} + \rho(\vec{V} \cdot \nabla)\vec{V} = -\nabla p + \mu \nabla^2 \vec{V} + \rho \vec{g}\beta(T_o - T) + \rho \vec{f} \qquad (4.6)$$

Since the equations on the Navier-Stokes set are coupled, when solving them using Boussinesq approximations, they must be solved simultaneously. For iterative solution algorithm for the fluid set in Equations 4.1, 4.2, and 4.3 a formulation must ensure coupled satisfaction of all the equations at convergence. The pressure-correction [61] or velocity-correction [62] schemes can also be used to arrive at an iterative solution algorithm. Here shown, the velocity-correction scheme is adopted. First an initial velocity condition that satisfies the continuity equation is proposed such that

$$\nabla \cdot \overrightarrow{V}^{(0)} = 0 \tag{4.7}$$

And then, from the Navier-Stokes, the estimation of a new velocity field $\overrightarrow{V}^{(*)}$ may be estimated by positioning the space operators at the current time step by

$$\rho \frac{\partial \overrightarrow{V}^{(*)}}{\partial t} = -\nabla p^{(k)} + \mu \nabla^2 \overrightarrow{V}^{(k)} + \rho(\overrightarrow{V}^{(k)} \cdot \nabla)\overrightarrow{V}^{(k)} + \rho \overrightarrow{g} \beta(T_o - T^{(k)}) + \rho \overrightarrow{f} \tag{4.8}$$

The equation proposed above can be advance using a backward-difference approximation of the time derivative in a single or multistep scheme. From here, the new velocity can determined from the boundaries by setting the conditions of the form

$$\partial \frac{\partial \overrightarrow{V}^{(*)}}{\partial t} + \eta \frac{\partial \overrightarrow{V}^{(*)}}{\partial \eta} + \gamma \overrightarrow{V}^{(*)} = \sigma \tag{4.9}$$

Equation 4.9 is the solution of Equation 4.8 but is does not satisfies the continuity equation. However, it can be accomplished if the velocity field is updated with a velocity variation field as

$$\overrightarrow{V}^{(k+1)} = \overrightarrow{V}^{(*)} + \delta \overrightarrow{V} \tag{4.10}$$

Also for irrotational velocity fields, a potential can be proposed using a Helmholtz correction potential of the form

$$\nabla \Phi \equiv -\delta \overrightarrow{V} \tag{4.11}$$

It can also be shown that a Poisson equation can be used, if the velocity field is required to satisfy continuity such that

$$\nabla^2 \Phi = \nabla \overrightarrow{V}^{(*)} \tag{4.12}$$

And it can be solved by converting it into a diffusion equation using artificial diffusivity

$$\frac{1}{\alpha_\Phi} \frac{\partial \Phi}{\partial t} = \nabla^2 \Phi - \nabla \cdot \overrightarrow{V}^{(*)} \tag{4.13}$$

Using convergence, this last equation can be artificially stepped until convergence using fractional time-stepping starting from the Helmholtz potential field and by imposing a complete set of homogeneous boundary conditions. After applying boundary conditions, the velocity field is updated and forced to satisfy continuity such that

$$\overrightarrow{V}^{(k+1)} = \overrightarrow{V}^{(*)} - \nabla \Phi \tag{4.14}$$

To update the pressure field, the divergence of the momentum equation is taken and by applying the continuity equation the following expression is derived

$$\nabla^2 p^{(k+1)} = \rho \nabla \cdot \left[\overrightarrow{g} \beta (T_o - T^{(k)}) + \overrightarrow{f} - (\overrightarrow{V}^{(k+1)} \cdot \nabla) \overrightarrow{V}^{(k+1)} \right] \tag{4.15}$$

This equation can be solved by converting it into a diffusion equation using artificial diffusivity to arrive at an expression of the form

$$\frac{1}{\alpha_p} \frac{\partial p}{\partial t} = \nabla^2 p - \rho \nabla \cdot \left[\overrightarrow{g} \beta (T_o - T^{(k)}) + \overrightarrow{f} - (\overrightarrow{V}^{(k+1)} \cdot \nabla) \overrightarrow{V}^{(k+1)} \right] \tag{4.16}$$

Using the same fractional time-stepping for the momentum equation starting from a pressure field p_k obtained at the previous real time step and by imposing a proper and complete set of boundary conditions generalized derived from Navier-Stokes equation , this

equation can be artificially stepped until convergence. The proposed equation has the following form

$$\eta \frac{\partial p^{(k+1)}}{\partial n} + \gamma p^{(k+1)} = \sigma \tag{4.17}$$

With the updated velocity field, the temperature field can be solved from Equation 4.3 using an explicit scheme such that

$$\rho c \frac{\partial T^{(k+1)}}{\partial t} = k \nabla^2 T^{(k)} - \rho c (\overrightarrow{V}^{(k+1)} \cdot \nabla) T^{(k)} + \Phi^{(k+1)} \tag{4.18}$$

Equation 4.18 can be marched in time using the same fractional time-stepping scheme used for the momentum equation starting from an initial temperature field and imposing boundary conditions.

These set equations can be iterated within each time step for time-accurate solution or can be stepped once through the domain if only steady-state solutions are needed.

4.2   Formulation of Boundary Conditions

Once the governing equations have been stated, the next step is to establish and define the right set of boundary conditions for the problem in hand. As it was observed in the last section, the set of differential equations to solve the problem in hand are fully coupled. Therefore boundary conditions to solve for all the fields need to be formulated. The following are typical boundaries used to solve these equation.

- Boundary conditions for $\overrightarrow{V}$

    1. Inlet (Prescribed Velocity) $\overrightarrow{V} = \hat{V}$

2. Slip Wall $\hat{V} = 0$

3. Outlet $\phi = 0$

- Boundary conditions for ϕ

  1. Inlet (Prescribed Velocity) $\frac{\partial \phi}{\partial n} = \hat{V}$

  2. Slip Wall $\frac{\partial \phi}{\partial n} = 0$

  3. Outlet $\phi = 0$

- Boundary conditions for p

  1. Inlet $\frac{\partial p}{\partial n} = [\mu(\nabla^2 \overrightarrow{V}) - \rho\frac{\partial \overrightarrow{V}}{\partial t} + \rho\overrightarrow{g}\beta(T_o - T) + \rho\overrightarrow{f}] \cdot \hat{n}$

  2. Wall $\frac{\partial p}{\partial n} = [\mu(\nabla^2 \overrightarrow{V}) - \rho\frac{\partial \overrightarrow{V}}{\partial t} - \rho(\overrightarrow{V} \cdot \nabla)\overrightarrow{V} + \rho\overrightarrow{g}\beta(T_o - T) + \rho\overrightarrow{f}] \cdot \hat{n}$

  3. Outlet $p = \hat{p}$

- Boundary conditions for T

  1. Forced $T = \hat{T}$

  2. Natural $k\frac{\partial T}{\partial n} = -\hat{q}$

  3. Convective $k\frac{\partial T}{\partial n} = -h(T - T_{ref})$

  4. Outlet $\frac{\partial T}{\partial t} + V_n\frac{\partial T}{\partial n} = 0$

Where, $\hat{V}$, $\hat{p}$, $\hat{T}$, $\hat{q}$, and h are prescribed values to initialize the problem. $\hat{V}_n$ is the normal velocity and the derivative with respect to the outward-drawn normal is prescribed by $\partial/\partial n$. Using the Helmholtz decomposition approach over the standard pressure-correction scheme gives more stability since the domain is being solved for the pressure field in each iteration instead of simply doing a correction.

4.3 Environment modeling

Having develop the concepts underlying the LRBF methods, governing equations, and boundary conditions. it is now appropriate to demonstrate the ability of the mentioned techniques to properly represent a EEIE and solved the heat transfer problem. Figure 4.1 provides the representation of the domain where it can clearly been that is composed by two regions. The first region is given by the insulation wall, which will be one of the parameters that will be change for each scenario. Three different materials will be used to look at the variations of temperature within time. Also is important to notice that there will be an applied heat flux in the outside wall which will quantify the effects of convective and radiation heat transfer. Is also important to mention that the heat transfer from the outside wall to the room is purely governed by conduction.
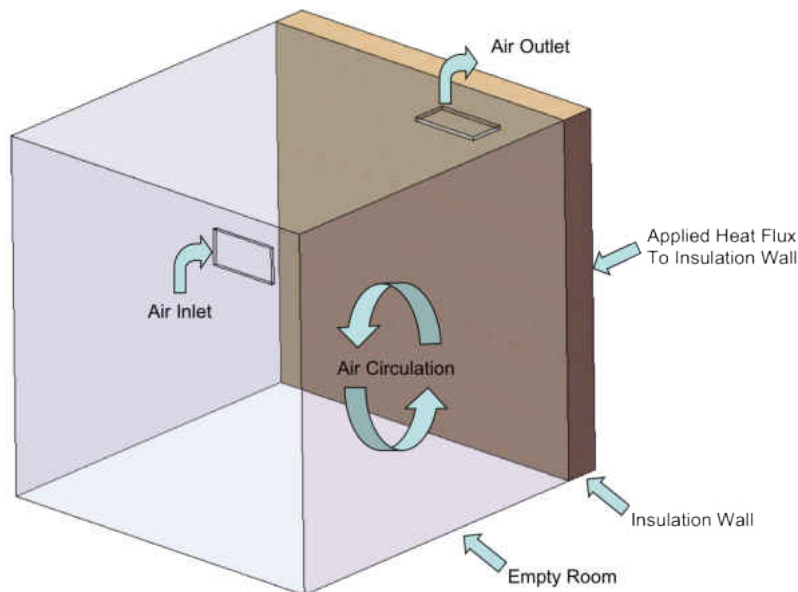

Figure 4.1: EEIE Representation

The heat flux to be applied to the insulation wall on the outside will be an average of the heat transfer due to convection and radiation. It will be quantify from $100\ W/m^2$ to $1000\ W/m^2$ in an period of 5 hours.

The second region is modeled as an empty room where air will be circulating. The mentioned room will have one air inlet, which will be the analogy of having an air conditioning inlet where the temperature will be kept constant at 75 F during the whole process. The mass flow rate given for a standard process with the given conditions and it is found in the literature [63] to be 0.221 kg/s. Also an air outlet will be modeled as a pressure outlet where the air is assumed to be discharged to the atmosphere in order to have air circulation to maintain a comfortable temperature inside the room. As already mentioned on this particular region there are interesting effects happening due to natural and force convection.

As it was mentioned in the formulation of the governing equations, a natural convection flow field is a self sustained flow drive by the presence of a temperature gradient as opposed to forced convection flow where external means are used to provide the flow. Due to this temperature difference, the density field is not uniform and buoyancy will induce a flow current due to the gravitational field and the variation in the density field. Because of the small mass flow and the big scale of the room, the problem in hand will be dominated by natural convection instead of forced convection.

The RLBF meshless method as already mentioned is a robust method and it has been tested [3] against commercial software for different scenarios where natural and forced convection is present giving not only accurate results but also reducing computational time for these type of strong coupled problems.

Figure 4.2 shows a 2D representation of the problem field with the regions previously described. It also shows standard dimensions for the construction of the insulation insulation wall, inlets, and outlets. This particular geometry will be used to solve the problem by using the RLBF meshless and the governing equations.
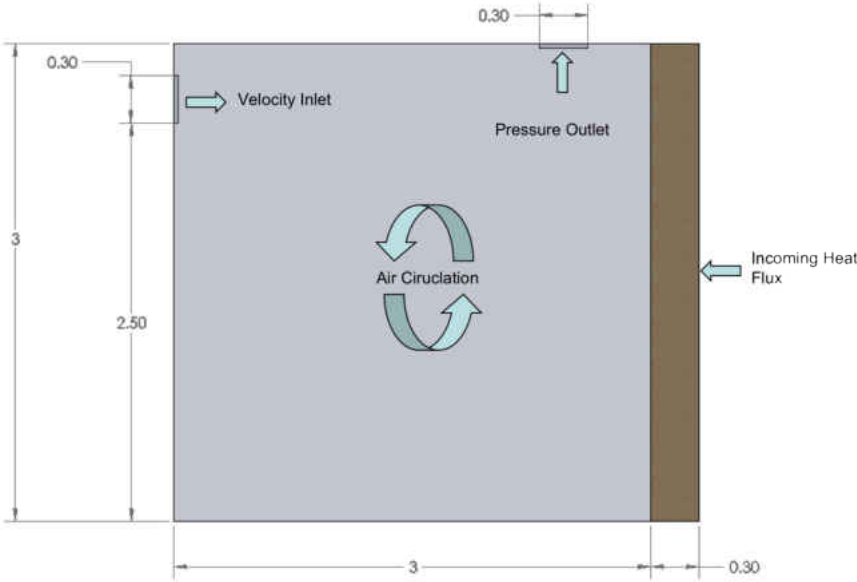

Figure 4.2: 2D Representation of EEIE

Due to all the physical effect mentioned before, it is expected to have air circulation. Also depending on the thermal conductivity of each different material used, a different thermal profile will be developed. The purpose at the end of the day is to calculate an average temperature inside the room at each time step to see the fluctuations of air depending on the material used for each simulation. The following section will resume the results after quantifying all the result obtained.

CHAPTER 5
RESULTS

The previous chapter has shown the development of the problem in hand focusing in the implementation of LRMF meshless method and the theory behind the use of biomaterials as thermoregulatory construction materials. After describing in detail the entire process of the developing and modeling the environment of our study, this chapter will now present the quantification of the results. These results are obtained using the configuration well described in the previous chapter. The quantification of the results will illustrate the benefits of using different configuration of materials when designing EEIE. As it was mentioned before the analysis will be marching in time for 5 hours. During these 5 hours a variable heat flux due to convective and radiation heat transfer will be imposed in the insulations wall. For the insulation wall three different materials have been selected to demonstrate the effects of using a diversity of materials will improve the insulation due to the different values of thermal conductivity in each scenario. For this particular study the selected materials are dry clay, granite, gravel concrete, concrete, and carbon steel. all the physical properties of these materials have been taken at ambient temperature. These results also provide date needed for several important comparisons, including material selection when designing EEIE and temperature fluctuations which will determine power consumption on these type of environments. The clay example shows the real applicability of this research in a real life application since the quantification of these results will determine its performance

and advantage not only as a construction material but also as a thermoregulatory organic material.

After applying the respective boundary conditions to the model, the results are presented in marching in time. Figure 5.1 shows the temperature profile and the velocity vectors after 1.25 hours.
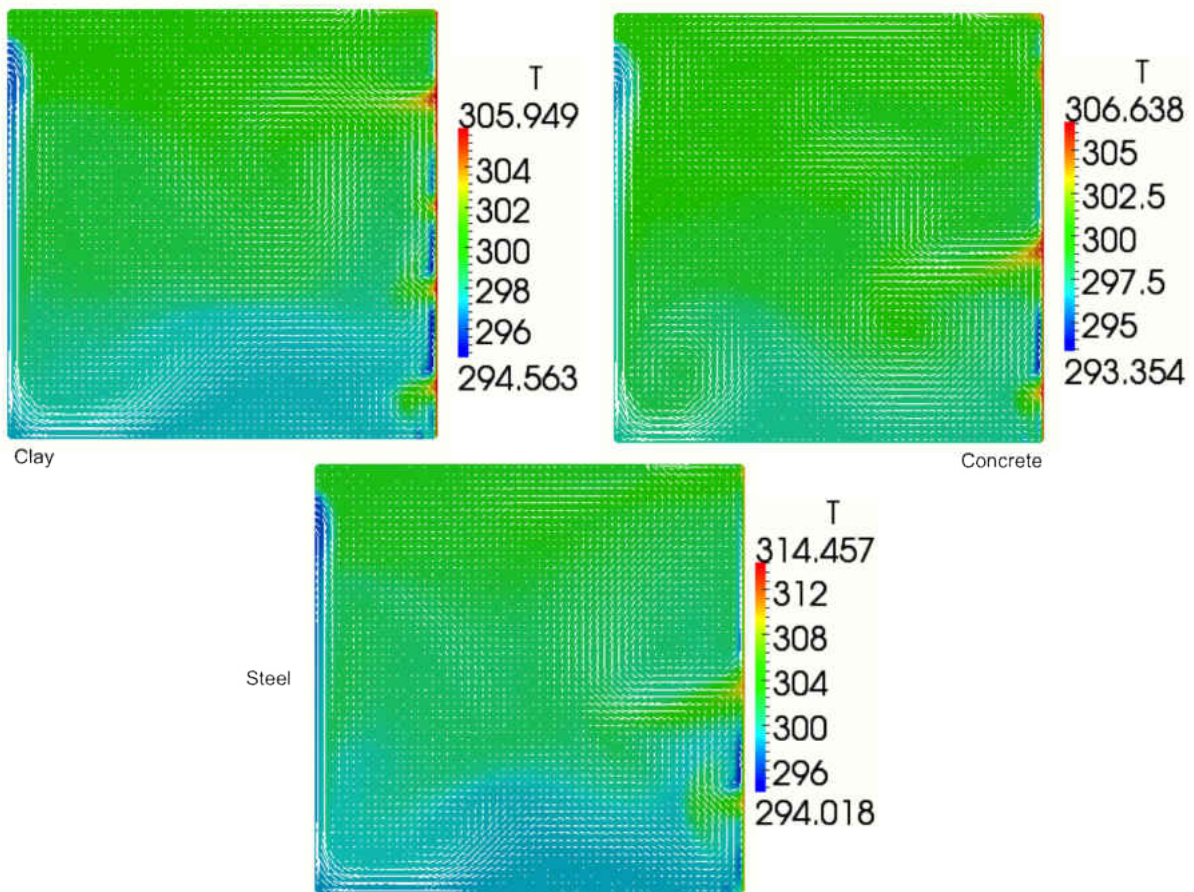

Figure 5.1: Temperature contours and velocity vectors after 1.25 hours

On these preliminary result it can clearly be seen that after 1.25 hours the average temperature where the clay was used as the insulation material the average temperature is less than in the other materials. Also as it was expected the airflow is buoyancy driven

and natural convection dominates over the force convection imposed at the inlet. Figure 5.2 shows the results at 2.5 hours.
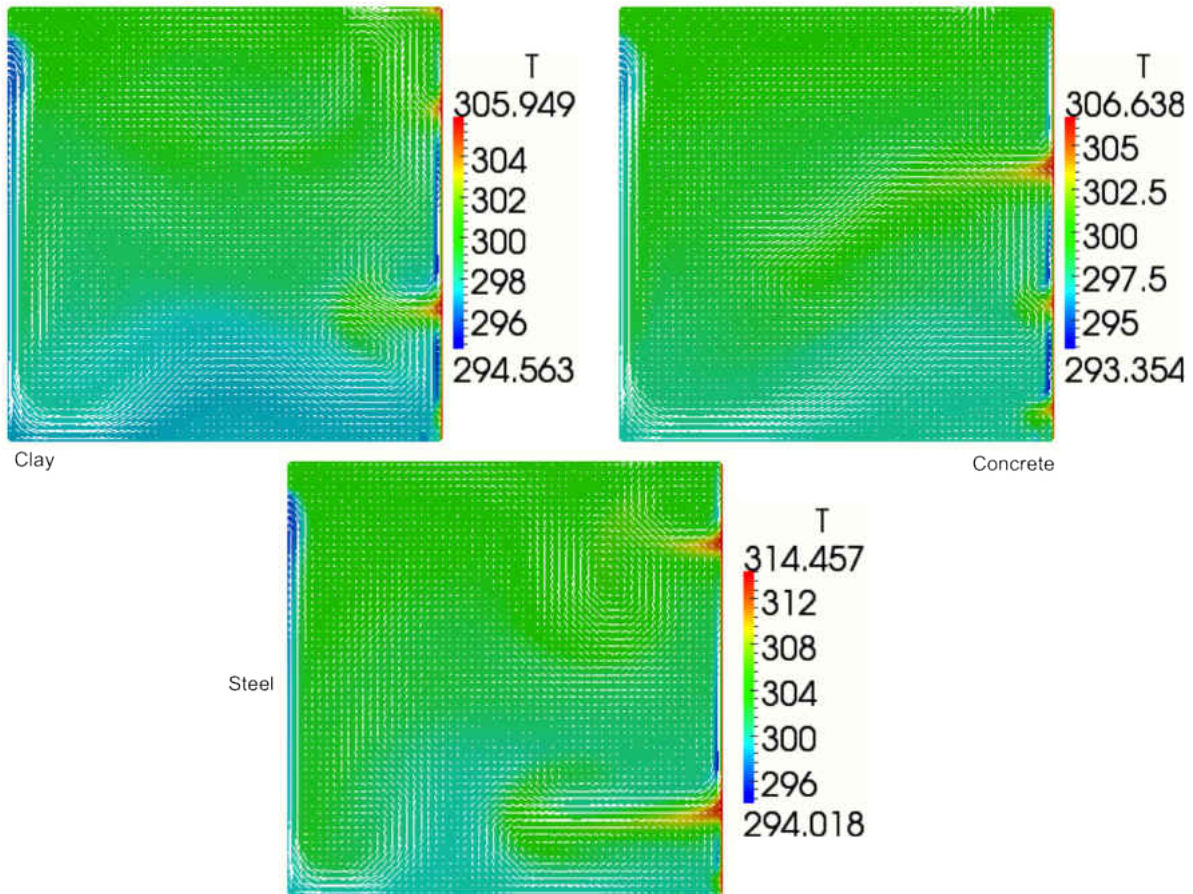

Figure 5.2: Temperature contours and velocity vectors after 2.5 hours

On this particular figure it is observed that still the average temperature is less that in the other model but also it can be seen that due to the high conductive of the carbon steel, the average temperature starts to rise at a much bigger rate when comparing to the other two scenarios. It is also concluded that from this point on the average temperature will be out of the "comfort zone" which is lies between 291 K and 305K. From this point on the

result will be only presented for the dry clay and the concrete since the carbon steel failed to meet the requirements of the design.

As the heat flux keeps on increasing due to convective and radiation effects, Figure 5.3 still shows that the average temperature in the clay environment is less than in the concrete environment. Also is noticed that the fluctuations of temperature are less in the clay environment, which will increase energy efficiency in real world construction applications.
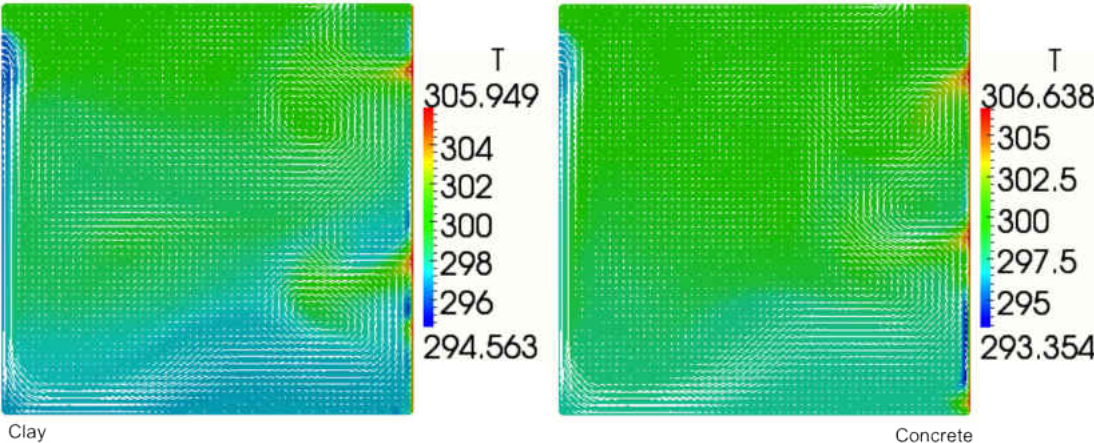

Figure 5.3: Temperature contours and velocity vectors after 3.75 hours

After 5 hours when the heat flux reaches its peak value of $1000 \, W/m^2$, which represents a very hot day in Florida, it can be still observed in Figure 5.4 that the average temperature in the clay environment is less than in the concrete environment. At this point there is a clear indication that the clay environment has a better performance than the concrete environment when it comes to maintaining fewer fluctuations of temperature.
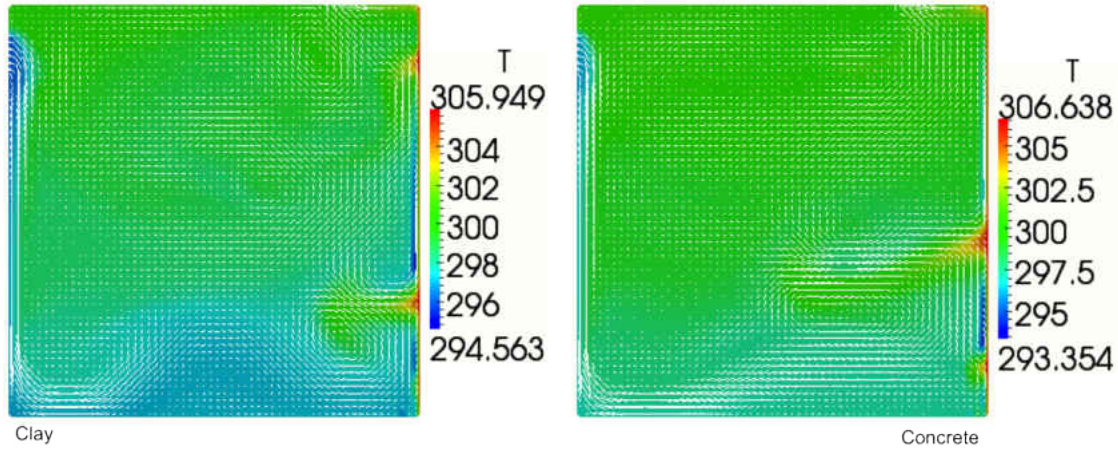
Figure 5.4: Temperature contours and velocity vectors after 5 hours

Table 5.1 shows the values of average temperature in 5 hours. Again these values will show that Clay is not only a great construction material but also it has the advantage to improve cooling effects under convective and radiation effects. Its behavior is very stable in time and does not fluctuate as much as in the case of the concrete environment. Also it is noticed that the carbon steel is out of the desired range but was included in the analysis in order to quantify the effects on these types of metal materials.

Table 5.1: Average Temperature in 5 hours

Average Temperature (K)	1 hour	2 hours	3 hours	4 hours	5 hours
Clay	298.84	298.79	298.62	298.63	298.62
Concrete	298.94	298.88	298.81	298.82	298.96
Concrete/Gravel	299.05	299.15	299.65	300.82	302.22
Granite	299.12	299.25	300.92	302.25	205.26
Carbon Steel	300.38	301.97	304	306	308

Lastly, Figure 5.5 shows the fluctuations of the average temperature in all the environments with time. This plot show that even if the values for the clay environment and the concrete are very close, the fluctuations of temperature are less in the clay, which at the end improve energy efficiency. Due to the large value of thermal conductivity, the carbon steel failed to be including in the possible list of materials that can be used in the designing of EEIE.
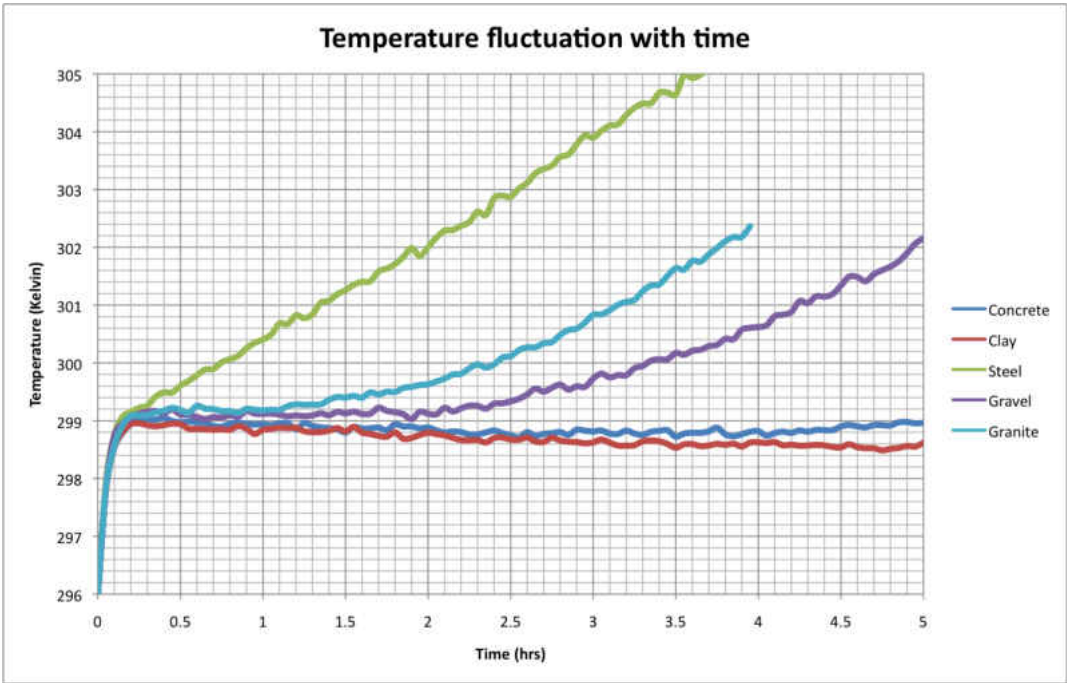

Figure 5.5: Temperature Fluctuations

CHAPTER 6
CONCLUSIONS AND FUTURE WORK

In conclusion, this thesis has introduced to use of RLBF meshless method in the designing of EIEE. This technique has already been proven and used successfully in many applications and has been proved to predict average temperature fluctuation and also to test the thermal efficiency in the designing of EEIE. As it was explained the fluid flow is modeled as an incompressible buoyancy driven solve thorough the Boussinesq approximation. After developing the corresponding governing equations and applying the correct boundary conditions, the solver predicted that out the diverse selection of material dry clay is the best option to solve the efficiency problem in EIEE. Dry clay provided the least amount of fluctuations through the time of the analysis, which will drastically reduce the amount of power consumption in large periods of time. This work has provided preliminary results on the designing of EEIE using a two-dimensional geometrical configuration, which leave the door open to new applications and future development. Future wok might introduce the extension from a two-dimensional to a three-dimensional geometrical configuration. Lastly, with the present availability of manufacturing custom materials, a new application could be found in the area of shape and material properties optimization by applying existing optimization methods such as genetic algorithms. In the same fashion as the RLBF meshless method was implemented, a systematic computational optimization study could be conducted based on objective functions aimed at arriving at composites of renewable earth-based materials that

mimic the properties and thermal regulation mechanisms of biological skin tissue. To solve this type of problem the domain material composition and geometrical configuration can be automatically adjusted until a targeted transient temperature distribution is achieved within the enclosed space. By using an optimization process, new material can be reverse engineer to provide nearly perfect thermal regulators.

LIST OF REFERENCES

[1] Liu, G.R., *Mesh Free Methods: Moving Beyond the Finite Element Method*, CRC Press, Boca Raton (2002).

[2] Chung, T.J., *Computational Fluid Dynamics*, Cambridge University Press (2000).

[3] Divo, E. and Kassab, A., "Localized Meshless Modeling of Natural Convective Viscous Flows", *Numerical Heat Transfer, Part A: Fundamentals*, **53**(6), 487–509 (2008).

[4] Divo, E. and Kassab, A., "Modeling of Convective and Conjugate Heat Transfer by a Third Order Localized RBF Meshless Collocation Method", in "Proceedings of NHT-05, Eurotherm82", (2005).

[5] Divo, E. and Kassab, A., "An Efficient Localized RBF Meshless Method Applied to Fluid Flow and Conjugate Heat Transfer", in "ASME IMECE", (2005).

[6] Beek, V. and W., G., *Glorious Mud*, Rowman & Littlefield Publisher (2007).

[7] Minke, G., *Earth Construction Handbook*, WIT Press, Boston (2000).

[8] Minke, G., *Building with EARTH*, Birkhauser-Publisher for Architecture (2006).

[9] Laurence, K., *Earth Building: Methods and Materials, Repair and Conservation*, Taylor & Francis (2005).

[10] H.Fathy, *Natural Energy and Vernacular Architecture: Principles and Examples with Reference to Hot Arid Climates*, United Nation University by the University of Chicago Press (1986).

[11] Singh, M.K., Mahapatra, S. and Atreya, A.K., "Thermal Performance Study and Evaluation of Comfort Temperatures in Vernacular Buildings of North-East India", *Building and Environment*, **45**(2), 320–329 (2010).

[12] Goodhew, S., Griffiths, R., Watson, R. and Short, D., "Some Preliminary Studies of the Thermal Properties of Devon Cob Wall", in "8th International Conference on the Study and Conservation of Earthen Architecture", 129–143, Terra (2000).

[13] Laird, D.A., "Layer Charge Influences on the Hydration of Expandable 2:1 Phyllosilicates", *Clays and Clay Minerals*, **47**(5), 630–636 (1999).

[14] Ju, Z., Ren, T. and Horton, R., "Influences of Dichlorodimethylsilane Treatment on Soil Hydrophobicity, Thermal Conductivity, and Electrical Conductivity", *Soil Science*, **173**(7), 425–432 (2008).

[15] Lipiec, J., Usowicz, B. and Ferrero, A., "Impact of Soil Compaction and Wetness on Thermal Properties of Sloping Vineyard Soil", *International Journal of Heat and Mass Transfer*, **50**(19-20), 3837–3847 (2007).

[16] Campbell, G.S., *An Introduction to Environmental Biophysics*, Springer-Verlag, New York (1977).

[17] Taiz, L. and Zeiger, E., *Plan Phisiology*, Sinauer Associates, Inc., Massachusetts (2002).

[18] Ibanez, M. and Castellvi, F., "Simplifying Daily Evapotranspiration Estimates over Short Full-Canopy Crops", *Agronomy Journal*, **92**, 628–632 (2000).

[19] Asasutjarit, C., Hirunlabha, J., Khedarid, J., Charoenvaia, S., Zeghmatib, B. and Shinc, U.C., "Development of Coconut Coir-based Lightweight Cement Board", *Construction and Building Materials*, **21**, 277–288 (2007).

[20] Pillai, C.K.S., Satyanarayana, M.A.V.K.G., Sreedharan, V.P., Indira, C. and Rohatgi, P.K., "A Mechanical Study of the Deterioration of Coconut Leaf Thatch under Natural and Accelerated Environmental Conditions", *Materials Science*, **17**(10), 2861–2868 (1982).

[21] Bilba, K., Arsene, M.A. and Ouensanga, A., "Study of Banana and Coconut Fibers: Botanical Composition, Thermal Degradation and Textural Observations", *Bioresource Technology*, **98**(1), 58–68 (2007).

[22] Olorunnisola, A.O., Pitman, A. and Mansfield-William, H., "Hydration Characteristics of Cement-bonded Composites made from Rattan Cane and Coconut Husk", *Journal of Bamboo and Rattan*, **4**(2), 193–201 (2005).

[23] Gatenby, R.M., "Exponential Relation Between Sweat Rate and Skin Temperature in Hot Climated", *Agricultural Science*, **106**, 175–183 (1986).

[24] Colin, J. and Houdas, Y., "Initiation of Sweating in Man After Abrupt Rise in Environmental Temperature", *Applied Phisiology*, **20**, 984–990 (1965).

[25] Wurster, R.D. and McCook, R.D., "Influence of Rate of Change in Skin Temperature on Sweating", *Applied Phisiology*, **27**(2), 237–240 (1969).

[26] Shapiro, Y., Pandolf, K.B. and Goldman, R.F., "Predicting Sweat Loss Response to Excersice, Environment and Clothing", *European Journal of Applied Phisiology and Occupational Physiology*, **48**(1), 83–96 (1982).

[27] Malchaire, J.B., "Predicted Sweat Rate in Fluctuating Thermal Conditions", *European Journal of Applied Phisiology and Occupational Physiology*, **63**(3), 282–287 (1991).

[28] Choi, J.K., Lee, H.K., Park, Y.S. and Shiraki, K., "Effect of Uniform and Non-uniform Skin Temperature on Thermal Exchanges in Water in Humans", *International Journal of Biometeorology*, **47**(2), 80–86 (2003).

[29] Wakabayashi, H., Hanai, A., Yokoyama, S. and Nomura, T., "Thermal Insulation and Body Temperature wearing a Thermal Swimsuit During Water Inmersion", *Journal of Physiological Anthropology*, **25**(5), 331–8 (2006).

[30] Belytscho, T., Lu, Y. and Gu, L., "Element-Free Galerkin Nethods", *International Journal of Numerical Methods*, **37**, 229–256 (1994).

[31] Atluri, S. and Shen, S., "The Meshless Method", Tech. Science Press (2002).

[32] Atluri, S.N. and Zhu, T., "A New Meshless local Petrov-Galerking (MLPG) Approach in Computational Mechanics", *Computational Mechanics*, **22**, 117–127 (1998).

[33] Onate, E., Idehlson, S., Zienkiewicz, O.C., Taylor, R.L. and Sacco, C., "A Stabilized Finite Point Method for Analysis of Fluid Mechanics Problems", *Computer Methods in Applied Mechanics and Engineering*, **139**, 315–346 (1996).

[34] Melenk, J.M. and Babuska, I., "The Partition of Unity Finite Element Method: Basic Theory and Application", *Computer Methods in Applied Mechanics and Engineering*, **139**, 289–316 (1996).

[35] Gu, Y.T. and Liu, G.R., "Meshless Techniques for Convection Dominated Problems", *Computational Mechanics*, **38**, 171–182 (2006).

[36] Gottlieb, D. and Orzag, S.A., "Numerical Analysis of Spectral Methods: Theory and Applications", *Society for Industrial and Applied Mathematics* (1977).

[37] Maday, Y. and Quarteroni, A., "Spectral and Pseudo-Spectral Approximations of the Navier-Stokes Equations", *SIAM Journal of Numerical Analysis*, **19**, 761–780 (1982).

[38] Patera, A., "A Spectral Element Method of Fluid Dynamics: Laminar Flow in a Channel Expansion", *Computational Physics*, **54**, 468–488 (1984).

[39] Macaraeg, M. and Street, C.L., "Improvement in Spectral Collocation Discretization througha Multiple Domain Technique", *Applied Numerical Mathematics*, **2**, 95–108 (1986).

[40] Hwar, C.K., Hirsch, R., Taylor, T. and Rosenberg, A.P., "A Pseudo-Spectral Matrix Element Method for Solution of Three Dimensional Incompressible Flows and its Parallel Implementation", *Computational Physics*, **83**, 260–291 (1989).

[41] Fasshauer, G., "RBF Collocation Methods as Pseudo-Spectral Methods", in "Boundary Elements XVII", 47–57, WIT Press (2005).

[42] Powell, M.J.D., "The Theory of Radial Basis Function Approximation", in "Advances in Numerical Analysis", vol. II, 143–167, Oxford Science Publications, Oxford (1992).

[43] Buhmann, M.D., "Radial Basis Functions: Theory and Implementation", Cambridge University Press, Cambridge (2003).

[44] Dyn, N., Levin, D. and Rippa, S., "Numerical Procedures for Surface Fitting of Scattered Data by Radial Basis Functions", *SIAM Journal of Sci. Stat. Computing*, **7**(2), 639–659 (1986).

[45] Hardy, R.L., "Multiquadric Equations of Topography and Other Irregular Surfaces", *Geophysical Research*, **17**(8), 1905–1915 (1971).

[46] Kansa, E.J., "Multiquadrics- A Scattered Data Approximation Scheme with Application to Computational Fluid Dynamics I-surface Approximations and Partial Derivative Estimates", *Computers and Mathematics with Applications*, **19**, 127–145 (1990).

[47] Kansa, E.J., "Multiquadrics- A Scattered Data Approximation Scheme with Application to Computational Fluid Dynamics II-solutions to Parabolic, Hyperbolic, and Elliptic Partial Differential Equations", *Computers and Mathematics with Applications*, **19**, 147–161 (1990).

[48] Kansa, E.J., "Circumventing the Ill-Conditioning Problem with Multiquadric Radial Basis Functions: Applications to Elliptic Partial Differential Equations", *Computers and Mathematics with Applications*, **39**, 123–137 (2000).

[49] Franke, R., "Scattered Data Interpolation: Test of Some Methods", *Mathematics of Computation*, **38**, 181–200 (1982).

[50] Mai-Duy, N. and Tran-Cong, T., "Mesh-Free Radial Basis Function Network Methods with Domain Decomposition for Approximation of Functions and Numerical Solution

of Poisson's Equation", *Engineering Analysis with Boundary Elements*, **26**, 133–156 (2002).

[51] Cheng, A.H., Goldberg, M.A., Kansa, E.J. and Zammito, G., "Exponential Convergence and H-c Multiquadric Collocation Method for Partial Differential Equations", *Numerical Methods in P.D.E.*, **19**(5), 571–594 (2003).

[52] Ling, L. and Kansa, E.J., "A Least-squares Preconditioner for Radial Basis Functions Collocation Methods", *Advances in Computational Mathematics*, **23**, 31–54 (2005).

[53] Sarler, B. and Vertnik, R., "Local Explicit Radial Basis Function Collocation Method for Diffusion Problems", *Computers and Mathematics with Applications*, **51**(8), 1269–1282 (2006).

[54] Vertnik, R. and Sarler, B., "Meshless Local Radial Basis Function Collocation Method for Convective-Diffusive Solid-Liquid Phase Change Problems", *International Journal of Numerical Methods for Heat and Fluid Flow*, **16**(5), 617–640 (2006).

[55] Divo, E. and Kassab, A., "An Efficient Localized Radial Basis Function Meshless Method for Fluid Flow and Conjugate Heat Transfer", *ASME Journal of Heat Transfer*, **129**, 124–136 (2007).

[56] Divo, E. and Kassab, A., "Localized Collocation Meshless Method (LCMM) for Convectively Dominated Flows", Proceedings of the 8th World Congress on Computational Methods in Applied Sciences and Engineering, Venice, Italy (2008).

[57] Zahab, Z.E., Divo, E. and Kassab, A., "A Localized Collocation Meshless Method (LCMM) for Incompresible Flows CFD Modeling with Applications to Transient Hemodynamics", *Engineering Analysis with Boundary Elements*, **33**(8-9), 1045–1061 (2009).

[58] Divo, E., Kassab, A., Reddi, L., Kakuturu, S. and Hagen, S., "RBF-FVM Numerical Solution of the Poro-Elasticity Levee Problem with Time-Varying Boundary Condition", Proceedings of ECCOMAS Coupled Problems 2009, Ischia Island, Italy (2009).

[59] Divo, E. and Kassab, A., "A Meshless Method for Conjugate Heat Transfer", *Engineering Analysis*, **29**, 136–149 (2005).

[60] Divo, E., Mitteff, E. and Quintana, L., "A Parallel Domain Decomposition Technique for Meshless Methods Applications to Large-Scale Heat Transfer Problems", in "ASME Summer Heat Transfer Meeting", (2004).

[61] Patankar, S.V., *Numerical Heat Transfer and Fluid Flow*, Hemisphere, New York (1980).

[62] Harlow, F.H. and Welch, J.E., "Numerical Calculation of Time Dependent Viscous Incompressible Flow of Fluids with a Free Surface", *Physics of Fluids*, **8**, 2182–2189 (1965).

[63] Oko, C.O.C. and Diemuodeke, E.O., "Analysis of Air-conditioning and Drying Processes using Spreadsheet add-in for Psychrometric Data", *Journal of Engineering Science and Technology*, **3**, 7–13 (2009).